

# Latent Beam Diffusion Models for Decoding Image Sequences

Guilherme Fernandes<sup>1</sup>, Vasco Ramos<sup>1</sup>, Regev Cohen<sup>2</sup>, Idan Szpektor<sup>2</sup>, Joao Magalhaes<sup>1</sup>

<sup>1</sup>NOVA LINCS, NOVA School of Science and Technology, Portugal

<sup>2</sup>Google Research

jmag@fct.unl.pt, szpektor@google.com

## Abstract

While diffusion models excel at generating high-quality images from text prompts, they struggle with visual consistency in image sequences. Existing methods generate each image independently, leading to disjointed narratives — a challenge further exacerbated in non-linear storytelling, where scenes must connect beyond adjacent frames. We introduce a novel beam search strategy for latent space exploration, enabling conditional generation of full image sequences with beam search decoding. Unlike prior approaches that use fixed latent priors, our method dynamically searches for an optimal sequence of latent representations, ensuring coherent visual transitions. To address beam search’s quadratic complexity, we integrate a cross-attention mechanism that efficiently scores search paths and enables pruning, prioritizing alignment with both textual prompts and visual context. Human evaluations confirm that our approach outperforms baseline methods, producing full sequences with superior coherence, visual continuity, and textual alignment. By bridging advances in search optimization and latent space refinement, this work sets a new standard for structured image sequence generation.

## 1. Introduction

Image diffusion models [12, 42, 43] have made significant advancements in generating high-quality images. These models, especially when combined with text prompts, have shown great potential in producing detailed and contextually accurate visuals [29, 34, 37]. While they excel at generating individual images based on specific text prompts, they face challenges when it comes to creating coherent sequences of images. In most cases, each image is generated independently based on its own prompt, which does not naturally ensure visual continuity across multiple steps. This problem is further compounded when the narrative is non-linear, where a scene may be connected not only to the immediate prior scene but also to earlier scenes in the sequence. This dynamic can result in sequences that lack co-

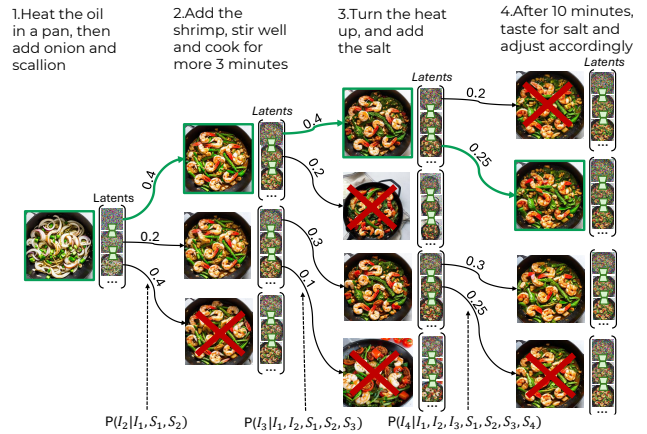


Figure 1. BeamDiffusion models leverage search in the latent denoising space for the best sequence of denoised images, where  $I_n$  represents the image at step  $n$  and  $S_n$  represents the text associated with step  $n$ .

herence and visual consistency over time [4].

We propose to utilize beam search as a potential solution to this problem. Beam search is a well-established technique in text generation tasks like machine translation [18, 21, 36, 47], allowing the model to explore multiple possible paths during the generation process, evaluating different trajectories and refining its predictions. However, despite its success in other domains, it has been barely explored in our context, leaving its potential untapped. In full image sequence generation, beam search could help navigate the complex latent space, refining coherence by adjusting text prompts or adding semantic cues.

In this work, we explore beam search for latent prior selection in image sequence generation. While previous research has used latent representations as priors to improve sequence consistency [4, 32], it remains unclear which specific representations yield the best overall sequence. We build on these ideas by introducing beam search to explore the latent space, enabling iterative refinement of image sequences. As illustrated in Figure 1, our approach leverages

search in the latent space to identify the best sequence of images, minimizing the risk of falling into suboptimal or incoherent paths, while maintaining visual continuity across images.

Due to the quadratic complexity of beam search algorithm, one needs to prune the search paths to keep a fixed number of candidate paths. To this end, we incorporate a cross-attention mechanism [23] that evaluates and scores candidate image paths based on their alignment with both the textual description of the next step and the visual context of previous steps. This provides a reliable quality measure for each path, allowing us to retain the best ones while pruning the least suitable, ensuring both adherence to instructions and visual continuity throughout the sequence.

We evaluated the effectiveness of our approach on three datasets: in the Recipes domain, and in the out-of-domain DIY Tasks and Visual Storytelling. Human evaluations show that our model outperformed baseline methods for generated sequence quality, showcasing its adaptability to diverse contexts.

## 2. Related Work

Decoding methods are essential for enhancing the quality of large language models (LLMs). Techniques such as beam search, top-k and nucleus sampling are widely studied for their effectiveness in balancing computational cost with generating coherent, contextually appropriate outputs [9, 13, 40]. Beam search has also proven effective in tasks like machine translation [27], image captioning [1, 19, 45], and visual storytelling [15]. Building on these ideas, our work innovates by applying beam search to explore the latent space in diffusion models for image sequence generation.

Ensuring coherence remains a significant challenge in multimodal sequence generation [6, 10, 20, 24]. Some approaches, like AR-LDM [28], encode the context of caption-image pairs into multimodal representations to maintain consistency across outputs. Similarly, Rahman et al. [31] incorporates the history of U-net [35, 38] latent vectors to preserve narrative coherence. However, these methods often face challenges such as computational inefficiency and the risk of noise propagation over time. Other approaches, such as Gill [22], combine LLMs with image encoder-decoder systems. While effective for certain tasks, these models suffer from alignment issues, with retrieved or generated images failing to match the narrative context, and they too often require complex training. Our method avoids these pitfalls by direct conditional generation against the guiding text while explicitly maintaining coherence via the beam search.

Interpreting diffusion models has become a focal point in recent research. Pont-Tuset et al. [30] anchor each word in textual descriptions to specific regions of images. Tang

et al. [44] analyze text-image interactions through cross-attention maps in the denoising module, offering insights into how textual prompts influence the generated images. Dewan et al. [7] enhance this interpretability by leveraging partial information decomposition to analyze how various components of a text prompt impact the generated image. In contrast, our beam-search approach focuses on generating images directly from textual input. Rather than mapping text to pre-existing images, it generates image sequences that are visually coherent and are consistently aligned with the evolving sequence of textual narrative.

Bordalo et al. [4] propose to use latent information from previous steps to guide coherent generation of subsequent images. However, their method relied on a greedy heuristic-based selection. CoSeD [32] improved on this idea and introduced a contrastive learning approach [5] to rank images generated from different latent seeds. Yet, both approaches focused on local refinements rather than optimizing across the entire sequence. Our beam search approach lifts these local selection criteria to perform global optimization.

## 3. Synthesis of Non-Linear Visual Sequences

In the following section, we define the challenges in image sequence generation, recall the core principles of LDM, Sec. 3.1, and then we detail BeamDiffusion key aspects in terms of diffusion beams (Sec. 3.2.1) and pruning (Sec. 3.2.2) with a contrastive approach (Sec. 3.2.3).

### 3.1. Problem Formulation

Generating a full sequence of visually coherent images from textual scene descriptions presents a challenge. Given a sequence of scenes  $S = \{s_1, s_2, \dots, s_L\}$ , where each scene  $s_j$  is a textual description, our goal is to generate a corresponding sequence of images  $\{I_1, I_2, \dots, I_L\}$  that maintain consistency across all steps.

Latent Diffusion Models (LDMs) [34] generate high-quality images in a compressed latent space. Instead of directly operating in pixel space, LDMs encode an input image  $I$  into a latent representation  $z$  using an encoder  $\mathcal{E}$  and reconstruct it through a decoder  $\mathcal{D}$  [2]. The U-Net backbone [35], denoted as  $\epsilon_\theta$ , incorporates a cross-attention mechanism [17] to condition the diffusion process on an external input  $\tau_\theta(s)$ , where  $s$  represents a textual prompt. LDMs are trained by minimizing:

$$L_{\text{LDM}} = \mathbb{E}_{\mathcal{E}(I), s, \epsilon \sim \mathcal{N}(0,1), t} [\|\epsilon - \epsilon_\theta(z_t, t, \tau_\theta(s))\|_2^2]. \quad (1)$$

While effective, LDMs generate images independently, starting from a randomly initialized latent  $z_T$ . This lack of temporal coherence makes it challenging to ensure consistency across generated sequences, especially in non-linear narratives [41], where maintaining character identity, lighting, and environmental details are crucial.

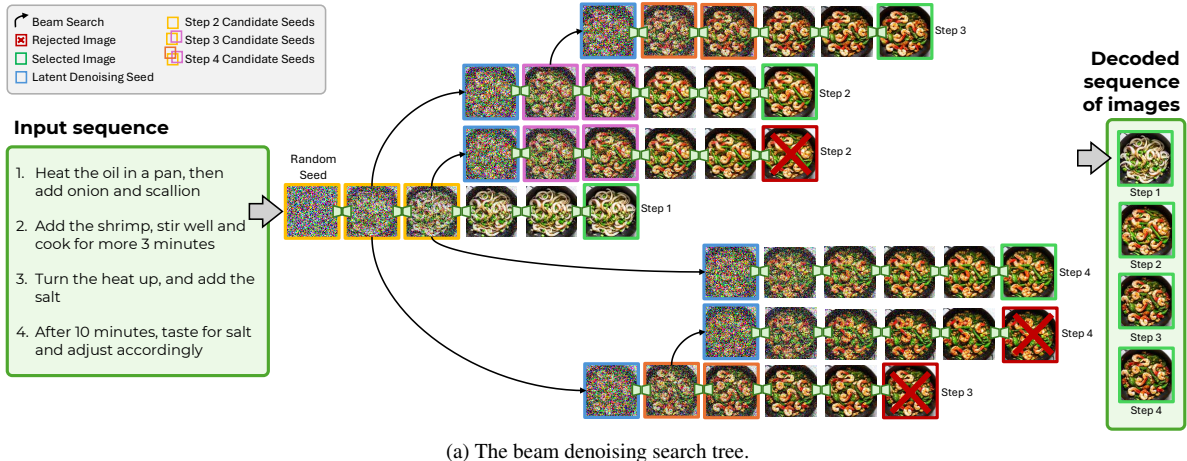


Figure 2. The BeamDiffusion model works in the denoising latent space by denoising the initial seed to latents and them decoding different beam paths. This shows how our method evolves in the latent space and how it can explore the latent space.

### 3.2. Beam Diffusion Model

To address the limitations of standard LDMs in generating coherent image sequences, we introduce the BeamDiffusion model. The proposed approach aims to enhance both the consistency and quality of image sequences by adopting a strategy inspired by beam search, but with a twist, it operates on latent denoising space. BeamDiffusion incorporates latent representations  $\mathcal{Z}_j$  from previously generated images. These latent representations guide the generation of new candidates, ensuring that each new image aligns with the context of the evolving sequence. This approach allows visual elements from previous images to be carried over or referenced, maintaining contextual consistency and continuity, while also adapting to the new scene description. In the following sections, we will detail the proposed method.

#### 3.2.1. Latent Space Exploration with Diffusion Beams

To maintain both diversity and coherence in the generated image sequence, we propose a diffusion-based exploration of the latent space across multiple steps. At each generation step  $j$ , the set  $\mathcal{I}_j = \{I_j^{(1)}, I_j^{(2)}, \dots, I_j^{(B)}\}$  consists of all possible candidate images, with  $I_j^{(b)}$  representing the image generated at step  $j$  for beam  $b$ .

**Sampling the Denoising Latent Space.** In the first step of the sequence,  $s_1$ , the model generates multiple candidate images using different random seeds. This approach

allows for a broader exploration of the latent space and reduces Bayes risk [3], as described in Appendix B. Hence, in this initial step,  $s_1$ , we obtain the first exploration samples from the denoising latent space, denoted as  $\mathcal{Z}_1 = \{z_1^{(1)}, \dots, z_1^{(K)}\}$ .

Building on prior work [4, 32], incorporating latent denoising from earlier steps ( $s_{<j}$ ) can enhance the denoising process. We define  $\mathcal{Z}_j$  to be the accumulation of latent representations from all preceding images up to step  $j$ :

$$\mathcal{Z}_j = \bigcup_{i \in \{j-n, \dots, j-1\}} \{z_i^{(1)}, \dots, z_i^{(K)}\}, \quad (2)$$

where each latent representation  $z_i^{(k)}$  corresponds to the  $k$ -th iteration of the diffusion process for image  $I_i$ . By utilizing latents from  $n$  previous stages (steps back), our approach ensures contextual consistency across generations.

Considering one particular search beam  $b$  in the latent space, to generate a new candidate image  $I_j^{(b)}$ , we condition the diffusion process on a latent representation  $z$  selected from the accumulated latents in  $\mathcal{Z}_j$ , as represented in Figure 2a. This conditional dependency is captured by the following probability expression:

$$p(I_j^{(b)} | \theta, z \in \mathcal{Z}_j, s_j), \quad (3)$$

where  $\theta$  are the model parameters. This formulation ensures that all denoising processes are correlated, as each new image  $I_j^{(b)}$  is generated based on latents  $z$  drawn from  $\mathcal{Z}_j$ . In

this way, each iteration in the denoising process acts as a seed for the next, establishing a dependency between successive denoising processes (Figure 2b).

**Diffusion Beams.** Following the idea of beam search, which maintains a set of the most promising candidates at each step and extends them sequentially [46], we construct diffusion beams by iteratively expanding candidate images. Formally, for each step  $j$ , we generate the set of all candidate images  $\mathcal{I}_j$  to compute the set of candidate diffusion beams  $\hat{B}_j$ . At the initial step  $j = 1$ , there are no previous beams to combine, so the initial set of beams can be represented as,

$$\hat{B}_1 = \bigcup_k \{I_1^{(k)} \mid I_1^{(k)} \in \mathcal{I}_1\}, \quad (4)$$

where  $\mathcal{I}_1$  is the set of initial candidate images generated using different random seeds indexed by  $k$ . For subsequent steps  $j > 1$ , each beam  $\hat{B}_{j-1}^{(b)}$  from the previous step is extended with new candidate images  $I_j^{(b,k)}$  from the set  $\mathcal{I}_j$ , and this extension is represented by the operator  $\oplus$ . The new set of beams is now represented as,

$$\hat{B}_j = \bigcup_{(b,k)} \left\{ \hat{B}_{j-1}^{(b)} \oplus I_j^{(b,k)} \mid I_j^{(b,k)} \in \mathcal{I}_j \right\} \quad (5)$$

where  $b$  is the index of a beam from the set  $\hat{B}_{j-1}$ , and  $k$  is the  $k$ -th latent variable from  $\mathcal{Z}_j$ . For each combination of a previous beam  $\hat{B}_{j-1}^{(b)}$  and latent  $\mathcal{Z}_j^{(k)}$ , the model considers a new candidate image  $I_j^{(b,k)}$  from the set of candidate images  $\mathcal{I}_j$ . The union over  $(b, k)$  combines all possible sequences of previous beams with the new candidate images, expanding the search space for the next step of generation.

### 3.2.2. Pruning Diffusion Beam Paths

Tracking diffusion beams helps maintain context and coherence across the growing image sequence by exploring multiple potential continuations. However, as the sequence progresses, focusing on the most promising paths within the beam budget (the number of beams that can be maintained simultaneously) becomes increasingly important to ensure the coherence of the generated images and optimize computational resources. To achieve this, our model prunes the diffusion beam paths, narrowing down the search space for the best candidates while promoting diversity and consistency in the maintained beams.

To prune candidate beams, the model scores each candidate  $\hat{B}_j$  by the likelihood of image  $I_j$  in the beam given the previous images  $I_{<j}$  and the step text. This is represented as  $p(I_j | s_j, B_{j-1}^{(b)})$ , where  $B_{j-1}^{(b)}$  represents the set of the most promising candidate beams from the previous step. Formally, the scoring is defined as:

$$\text{score}(\hat{B}_j^{(b)}) = \sum_{i=1}^j \log p(I_i | I_1, \dots, I_{i-1}, s_1, \dots, s_i), \quad (6)$$

where we sum the individual log-probabilities of each image in the sequence, reflecting the overall coherence and

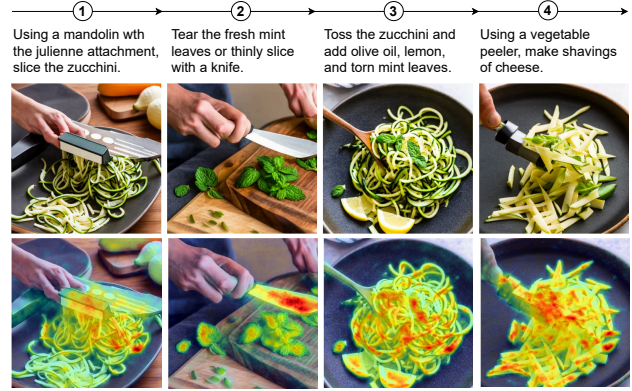


Figure 3. Visualization of cross-attention in latent diffusion, showing how BeamDiffusion focuses on different regions of the image based on the prompt at each stage. The heatmap highlights the areas with the strongest attention.

alignment with the context set by the previous images and prompts.

After scoring all candidate images in  $\mathcal{I}_j$ , the search space is refined by performing a beam search operation. This operation selects the most promising  $w$  diffusion beams, effectively limiting the beam width to  $w$ . The refinement process is expressed as,

$$B_j = \operatorname{argmax}_{B_j \subseteq \hat{B}_j, |B_j|=w} \left( \sum_{i=1}^w \text{score}(\hat{B}_j^{(i)}) \right) \quad (7)$$

where,  $B_j$  represents the most promising  $w$  candidate diffusion beams at the step  $j$ , ensuring that the updated beam evolves to explore the most promising options, guided by the previous context and the newly generated candidates, while maintaining a controlled beam width.

To maintain a broad search space in the early stages, pruning is delayed until after the second step. During this initial phase, all candidates are retained for exploration. After the second step, pruning is applied, limiting the candidates to the  $w$  most promising. This approach balances exploration and computational efficiency, focusing the model’s efforts on the most promising candidates in the later stages of generation.

### 3.2.3. Contrastive Score

While the basic pruning mechanism outlined above provides a foundation for selecting candidate images based on raw probabilities, the scoring function is now implemented as contrastive classifier. This classifier improves the image selection by learning from past sequences and aligning the candidates with the evolving context [32]. As illustrated in Figure 3, the heat maps show how BeamDiffusion attends to different regions of the input text at various stages, highlighting the evolving alignment between textual prompts and image features.

To compute these probabilities, we refine the approach using a softmax-based method to determine the likelihood of each candidate image  $I_j$  relative to all other possible candidates in the sequence. In this refined process, the probability  $p(I_j|s_j, B_{j-1}^{(b)})$  is replaced by the output of the classifier  $\varphi(I_j, s_j, B_{j-1}^{(b)})$ , which approximates the likelihood of each candidate fitting the sequence. The more detailed version of the scoring mechanism can be expressed as,

$$score(\hat{B}_j^{(b)}) = \sum_{i=1}^j \log \left( \frac{\exp(\varphi(I_i, s_i, B_{i-1}^{(b)}))}{\sum_{I'_i \in \mathcal{I}_i} \exp(\varphi(I'_i, s_i, B_{i-1}^{(b)}))} \right), \quad (8)$$

where the denominator in the softmax function normalizes the scores by summing over the candidate images  $I'_i$  for beam  $b$  within the set  $\mathcal{I}_i$ . This ensures that the score of selecting a particular candidate image  $I_j$  is computed relative to all other candidate images in the sequence, capturing how well it fits the overall sequence in terms of visual content and textual alignment.

**Training.** To train the classifier effectively, we employ a contextual sequence training approach, which enables the model to capture sequential relationships across different tasks. During training, the true label  $l_{t,j}$  indicates whether the candidate image  $I_j$  fits correctly into the sequence, given the previous steps  $B_{j-1}^{(b)}$  of the  $b$ -th beam. Here,  $t$  refers to the task index and  $j$  represents the step index within the sequence. The model’s prediction  $\varphi(I_j, s_j, B_{j-1}^{(b)})$  is based on the candidate image  $I_j$ , its textual description  $s_j$ , and the context provided by the prior steps. The model aims to minimize cross-entropy loss by aligning the candidate image with its context, ensuring it fits well within the sequence according to the true labels  $l_{t,j}$ , defined as:

$$\operatorname{argmin} \sum_{t=1}^M \sum_{j=1}^N l_{t,j} \log(\varphi(I_j, s_j, B_{j-1}^{(b)})) \quad (9)$$

Through contrastive training, the model learns to align representations of similar steps while enhancing the distinction between steps that differ semantically or visually.

### 3.2.4. Contextual Scene Descriptions

In many cases, step descriptions alone may lack context as precise visual prompts. These step descriptions are often interdependent, relying on prior steps for contextual understanding, or may miss visual details, e.g. *”Put the ice cream in freezer for 1 hour”*, or actions that involve multiple tasks, such as *”Slice the tomatoes, grate the cheese, and stir the sauce”*. To address this challenge, we leverage Gemini [33] to refine step descriptions into visually detailed prompts while considering sequence context. Specifically, Gemini produces a contextualized caption  $c_j$  based on the current step description  $s_j$  and all preceding steps as follows:

$$c_j = \phi(s_j | \{s_1, s_2, \dots, s_{j-1}\}) \quad (10)$$

Following this approach we can improve image generation prompts by maintaining consistency and preserving the dependencies between sequential steps. For further information, see Appendix E.

## 4. Experimental Setup

In this section, we describe the experimental setup to evaluate BeamDiffusion’s performance in generating coherent image sequences. We outline the datasets used, identify other baseline methods, and explain the human and Gemini evaluations focused on semantic and visual consistency across generated sequences. All data and implementations will be released after publication.

**Datasets.** We used a dataset consisting of publicly available manual tasks in the Recipes and DIY domains [4], as well as the Visual Storytelling (VIST) dataset [16]. Recipes serve as the in-domain dataset, while DIY tasks and VIST are out-of-domain. These out-of-domain datasets allow us to assess the generalizability of our model across different task domains. More details can be found in Appendix D.

**Baselines.** To assess the performance of our image sequence generation method for multistep tasks, we compared BeamDiffusion to two other decoding approaches, as well as GILL [22], focusing on different strategies for generating consistent image sequences:

- **Greedy/CoSeD<sub>len=1</sub>** [32]: In this method, a new image is generated at each step using the first five latents from the previous image, selecting the best overall image. Although similar to CoSeD<sub>len=1</sub>, it relies solely on CLIP without alterations, whereas CoSeD uses a trained module for selection.
- **Nucleus Sampling** [14]: Rather than choosing the single most likely image, nucleus sampling randomly selects from the set of images whose cumulative probability exceeds a specified threshold  $p$ , according to CLIP. This allows for more diversity in the generated sequence while still emphasizing high-probability outcomes.
- **GILL** [22]: Unlike the other methods, GILL does not explicitly search the latent space. Instead, it ensures coherent image sequences by iteratively generating images, while maintaining consistency across the sequence. GILL achieves this by deciding when to retrieve an image from a candidate set or when to generate a new image, based on the context of the previous images and text inputs.

**Human Evaluation.** In the first task, the annotators compared pairs of beam search configurations in a *”battle-style”* format to select which beam configuration was the best regarding beam width ( $w$  in 7) and steps back ( $n$  in 7). The winning configuration is compared against other

Method	Recipes		DIY		VIST	
	Human (%)	Gemini (%)	Human (%)	Gemini (%)	Human (%)	Gemini (%)
Greedy/CoSeD <sub>len=1</sub> [32]	13.3	16.7	20.0	10.0	27.2	16.7
Nucleus Sampling [14]	33.3	16.7	30.0	30.0	18.2	26.6
GILL [22]	0.0	3.3	10.0	20.0	0.00	0.0
BeamDiffusion	<b>53.3</b>	<b>63.3</b>	<b>40.0</b>	<b>40.0</b>	<b>54.5</b>	<b>56.7</b>

Table 1. Frequency of method selection by human annotators and Gemini.

configurations until a new configuration is selected as better. The selection criteria focused on semantic alignment and visual consistency. Semantic alignment assesses how well the image sequence matches the corresponding text, while visual consistency evaluates the coherence of the visuals across the sequence (e.g., keeping backgrounds, objects, or ingredients consistent).

Having chosen the optimal configuration, we need to assess how it compares to other methods. In the second annotation task, BeamDiffusion was compared with our baseline models. The annotators independently assessed the sequences, selecting the best method according to semantic and visual consistency, with the possibility of choosing multiple options or none. For further information, see Appendix C.

**Gemini Evaluation.** To further validate our findings and annotate a wider range of tasks, we used Gemini for both evaluation of configurations and baselines. Its selection process closely mirrored that of human annotators, with one key difference: Gemini tends to default to *“both good”* when given the option. To avoid this, we removed the *“both good”* and *“both bad”* options from its evaluation to ensure more accurate results.

We also refined our method for determining the best generation technique. Initially, presenting all four sequences at once caused the model to focus primarily on the last two, leading to biased results. To address this, we switched to pairwise evaluations, comparing sequences two at a time, which provided a more balanced and reliable assessment. For details, please refer to Appendix C.

**Human-Gemini Agreement.** We conducted an alignment assessment between human annotators and Gemini. We asked 10 annotators to rate 16 Recipes, 10 DIYs, and 10 VIST tasks. After this assessment, we computed Fleiss’ kappa [8], obtaining a value of 70%, indicating a substantial agreement. Given this substantial alignment, we extended the evaluation to the remaining sequences with Gemini.

## 5. Results and Discussion

In the following sections, we demonstrate the performance of BeamDiffusion and examine different aspects: hyperparameters, non-linear decoding properties and a qualitative analysis.

### 5.1. General Results

The results in Table 1 compare the performance of four methods, Greedy/CoSeD<sub>len=1</sub>, Nucleus Sampling, GILL, and BeamDiffusion, evaluated through human annotations and the Gemini model across three domains: Recipes (in-domain), DIY (out-of-domain), and VIST (out-of-domain).

Across domains, BeamDiffusion consistently outperforms other methods. In the Recipes domain, it leads with 53.3% in human evaluation and 63.3% in Gemini. Nucleus follows with 33.3% (human) and 16.7% (Gemini), while greedy scores 13.3% (human) and 16.7% (Gemini). In DIY, BeamDiffusion achieves 40.0% in both evaluations, again outperforming greedy and nucleus. In VIST, BeamDiffusion leads with 54.5% (human) and 56.7% (Gemini), with greedy and nucleus scoring significantly lower. GILL consistently underperforms, receiving 0% selection in VIST across both evaluations. In Recipes, it scores just 3.3% in Gemini and remains the weakest performer across all methods. While it performs slightly better in DIY, it still lags behind other approaches. Although BeamDiffusion excels in Recipes and VIST, performance in DIY remains more challenging, with smaller performance gaps between methods. This reflects the inherent complexity of the DIY domain, where generating coherent outputs is particularly difficult.

Overall, BeamDiffusion stands out as the most effective method across all domains, particularly in Recipes and VIST. However, its performance in DIY highlights the need for a more effective search in the latent space to ensure consistency and coherence across diverse tasks.

### 5.2. Best Beam Search Configuration

The hyperparameters beam width ( $w$  in Eq. 7) and steps back ( $n$  in Eq. 2), play a crucial role in the performance of BeamDiffusion. In this section, we evaluated different configurations across four beam widths (2, 3, 4, and 6) and three steps back (2, 3, and 4). In this study, we specifi-

Steps Back	Beam Width			
	2	3	4	6
2	8.33	8.33	<b>25.00</b>	8.33
3	<u>16.67</u>	-	-	-
4	<u>16.67</u>	8.33	8.33	-

Table 2. Influence of different hyperparameter values according to human annotations.

Steps Back	Beam Width			
	2	3	4	6
2	5.71	2.86	<b>48.57</b>	5.71
3	<u>28.57</u>	-	2.86	-
4	-	-	2.86	-

Table 3. Influence of different hyperparameter values according to Gemini annotations.

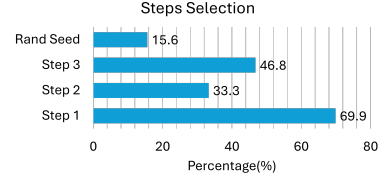


Figure 4. Non-linear steps selection, according to selection opportunities.

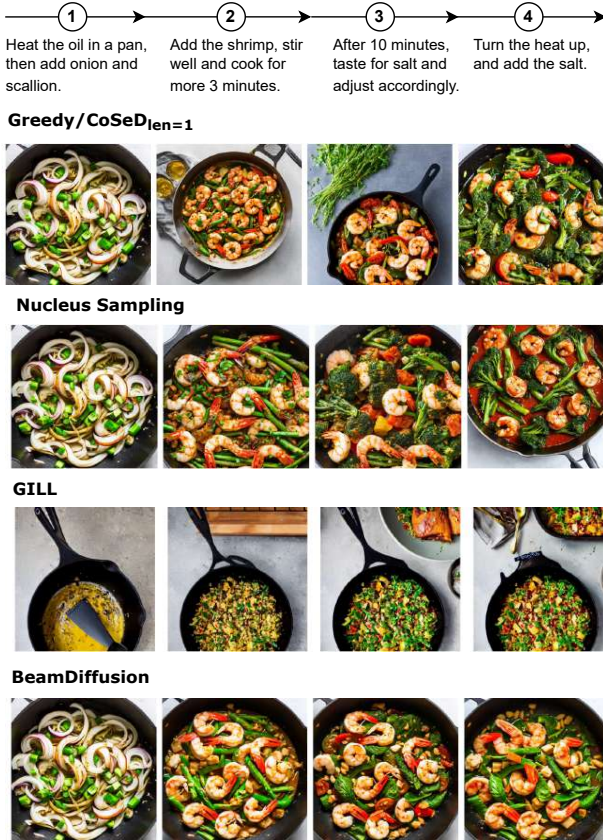


Figure 5. Example of the Recipes domain task "Jamaican Callaloo With Shrimp", with a sequence of 4 steps.

cally focus on latents indexes 0, 1, 2, and 3, denoted as  $K$  in Eq. 2, which yield the most promising results. A more detailed discussion on the impact of latents is provided in Appendix A.1.

We first performed human annotations on six tasks to identify the optimal beam search configuration, see Appendix C for details. The results in Table 2 showed that the best performing configuration was 2 steps back with a beam width of 4, achieving a selection rate of 25%. Other configurations, such as 3 steps back with a beam width of 2 and 4 steps back with a beam width of 2, also showed competitive performance (16.67%), but none outperformed the 2 steps back and beam width of 4 configuration. The con-

figurations with beam width 6 performed the worst in all the settings tested.

To assess the reliability of these findings, we used Gemini for the same evaluation on six tasks, achieving an 85% Fleiss' Kappa agreement [8], indicating near-perfect alignment. The results from the extended Gemini evaluation (Table 3) confirmed that the optimal configuration, 2 steps back with a beam width of 4, remained the best, now achieving a 48.57% selection rate, a significant improvement over the 33.33% from the initial six-task evaluation. Further, the configuration with 3 steps back and a beam width of 2 still performed well, yielding a 28.57% selection rate, confirming its robustness as an alternative. However, larger beam widths, such as beam width 6, continued to underperform, reinforcing that, in this task, a higher beam width does not always improve performance.

### 5.3. Non-Linear Sequence Denoising

To analyze how beam diffusion explore the latent space as formulated in Sec. 3.2.1, we examined the step from which the latent representation was selected during the generation process. For an analysis of latent selection, see Appendix A.2. We focused the step selection process in four-step sequences (Figure 4). Step 1 was chosen 69.9% of the time, highlighting its key role in shaping the sequence. Selection rates decrease for later steps, with Step 3 at 46.8% and Step 2 at 33.3%. The sum of these percentages exceeds 100% because they represent the relative selection frequency of each step, considering the number of possible selection opportunities. Earlier steps, such as Step 1, have more chances of being chosen, leading to a higher selection rate. Thus, the percentages reflect how often each step is selected given the different possibilities for their inclusion, rather than a simple additive total. This pattern demonstrates how beam search prioritizes crucial steps, particularly Step 1, to establish sequence coherence while strategically weighing intermediate stages. By balancing local accuracy with global consistency, BeamDiffusion ensures high-quality image sequences that remain visually and contextually aligned.

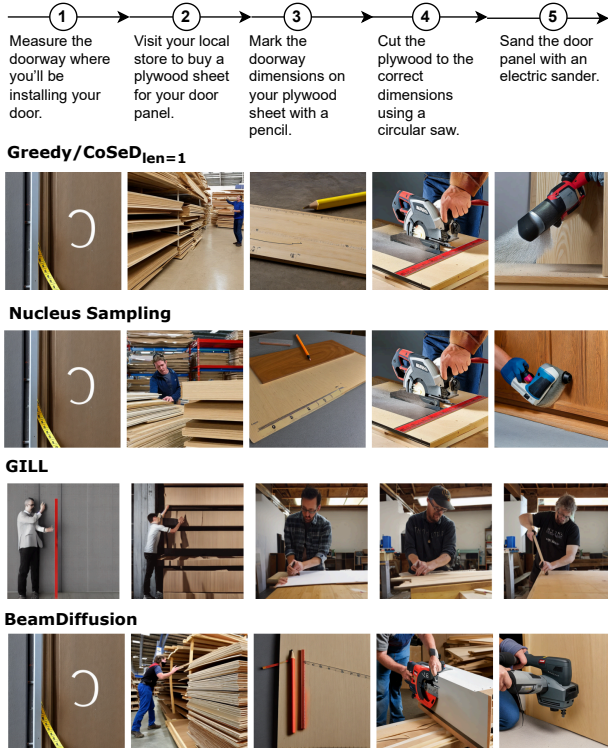


Figure 6. Example of the out-of-domain DIY task "How to Make a Door", with a sequence of 5 steps.

### 5.4. Qualitative Analysis

To illustrate how different decoding methods impact the semantic and visual consistency of generated output, we present several examples in Figures 5–7, and in Appendix F.2. In Figure 5, we see that BeamDiffusion consistently maintains the same pan across all steps, a quality not always achieved by greedy or nucleus methods. Meanwhile, GILL struggles to follow the text from step to step, leading to more inconsistencies in the outputs.

Looking at the out-of-domain DIY and VIST datasets, in Figure 6, we observe a task with intricate details. Although other methods fail to consistently capture the color of the plywood, BeamDiffusion outperforms by maintaining this detail, demonstrating its strength in preserving fine-grained elements in complex tasks. In Figure 7, we again observe significant inconsistencies with the greedy and nucleus methods, which alternate between black-and-white and color images. In contrast, BeamDiffusion keeps the color consistent throughout the sequence. Additionally, background elements, such as the bushes, remain stable across the first three steps. Even the persons in first step closely resemble those in the third, further emphasizing the BeamDiffusion consistency. At the same time, GILL consistently struggles to follow the text, failing to capture the necessary details.

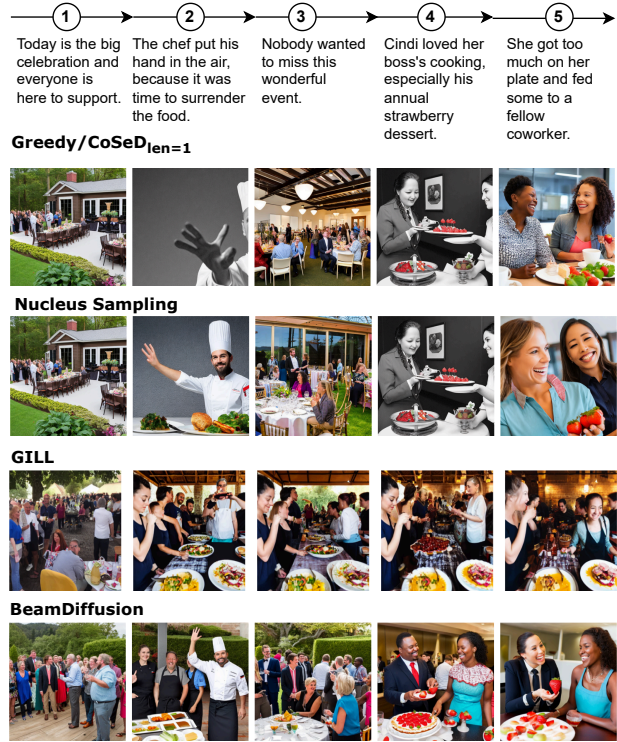


Figure 7. Example of the out-of-domain VIST story "July 4th Barbecue", with a sequence of 5 steps.

This analysis highlights BeamDiffusion ability to maintain high levels of semantic and visual consistency, even in out-of-domain tasks, much like its performance on Recipes.

### 6. Conclusions

In this paper, we proposed a novel method to explore the latent diffusion space with a beam search strategy, to generate image sequences. BeamDiffusion is a theoretically sound framework, drawing on the strengths of text-based decoding techniques [40], with clear experimental gains over alternative methods, as we demonstrated in generating image sequences with enhanced coherence and consistency.

Through both human and automatic evaluation, we show that beam search performs effectively in generating high-quality and coherent image sequences. The insights drawn from these evaluations reveal that beam search aligns closely with textual instructions while ensuring visual continuity. In contrast, GILL, the only method in our study that does not perform latent search, struggles to maintain consistent alignment with the text instructions, resulting in more inconsistent and less coherent image sequences. Furthermore, our results underscore the significance of the non-linear selection process in beam search, highlighting how prioritizing certain steps and latents can optimize the quality of the generation process.



## References

- [1] Shanmugasundaram Abinaya, Mandava Deepak, and A. Sherly Alphonse. Enhanced image captioning using bahdanau attention mechanism and heuristic beam search algorithm. *IEEE Access*, 12:100991–101003, 2024. 2
- [2] Dor Bank, Noam Koenigstein, and Raja Giryes. Autoencoders. *Machine learning for data science handbook: data mining and knowledge discovery handbook*, pages 353–374, 2023. 2
- [3] Amanda Bertsch, Alex Xie, Graham Neubig, and Matthew R. Gormley. It’s MBR all the way down: Modern generation techniques through the lens of minimum bayes risk. *CoRR*, abs/2310.01387, 2023. 3
- [4] João Bordalo, Vasco Ramos, Rodrigo Valerio, Diogo Glória-Silva, Yonatan Bitton, Michal Yarom, Idan Szpektor, and João Magalhães. Generating coherent sequences of visual illustrations for real-world manual tasks. pages 12777–12797, 2024. 1, 2, 3, 5, 12
- [5] Ting Chen, Simon Kornblith, Mohammad Norouzi, and Geoffrey Hinton. A simple framework for contrastive learning of visual representations. In *International conference on machine learning*, pages 1597–1607. PMLR, 2020. 2
- [6] Weifeng Chen, Jiacheng Zhang, Jie Wu, Hefeng Wu, Xuefeng Xiao, and Liang Lin. Id-aligner: Enhancing identity-preserving text-to-image generation with reward feedback learning. *arXiv preprint arXiv:2404.15449*, 2024. 2
- [7] Shaurya Dewan, Rushikesh Zawar, Prakanshul Saxena, Yingshan Chang, Andrew Luo, and Yonatan Bisk. Diffusionpid: Interpreting diffusion via partial information decomposition. *CoRR*, abs/2406.05191, 2024. 2
- [8] Joseph Fleiss. Measuring nominal scale agreement among many raters. *Psychological Bulletin*, 76:378–, 1971. 6, 7
- [9] Shaz Furniturewala, Kokil Jaidka, and Yashvardhan Sharma. Impact of decoding methods on human alignment of conversational llms. In *Proceedings of the 14th Workshop on Computational Approaches to Subjectivity, Sentiment, & Social Media Analysis, WASSA 2024, Bangkok, Thailand, August 15, 2024*, pages 273–279. Association for Computational Linguistics, 2024. 2
- [10] Michal Geyer, Omer Bar-Tal, Shai Bagon, and Tali Dekel. Tokenflow: Consistent diffusion features for consistent video editing. In *The Twelfth International Conference on Learning Representations, ICLR 2024, Vienna, Austria, May 7-11, 2024*. OpenReview.net, 2024. 2
- [11] Patrizia Grifoni and Patrizia Grifoni. *Multimodal Human Computer Interaction and Pervasive Services*. IGI Global, USA, 2009. 17
- [12] Jonathan Ho, Ajay Jain, and Pieter Abbeel. Denoising diffusion probabilistic models. *Advances in neural information processing systems*, 33:6840–6851, 2020. 1
- [13] Ari Holtzman, Jan Buys, Li Du, Maxwell Forbes, and Yejin Choi. The curious case of neural text degeneration. In *8th International Conference on Learning Representations, ICLR 2020, Addis Ababa, Ethiopia, April 26-30, 2020*. OpenReview.net, 2020. 2
- [14] Ari Holtzman, Jan Buys, Li Du, Maxwell Forbes, and Yejin Choi. The curious case of neural text degeneration. In *International Conference on Learning Representations*, 2020. 5, 6
- [15] Chao-Chun Hsu, Szu-Min Chen, Ming-Hsun Hsieh, and Lun-Wei Ku. Using inter-sentence diverse beam search to reduce redundancy in visual storytelling. *arXiv preprint arXiv:1805.11867*, 2018. 2
- [16] Ting-Hao K. Huang, Francis Ferraro, Nasrin Mostafazadeh, Ishan Misra, Jacob Devlin, Aishwarya Agrawal, Ross Girshick, Xiaodong He, Pushmeet Kohli, Dhruv Batra, et al. Visual storytelling. In *15th Annual Conference of the North American Chapter of the Association for Computational Linguistics (NAACL 2016)*, 2016. 5
- [17] Andrew Jaegle, Felix Gimeno, Andy Brock, Oriol Vinyals, Andrew Zisserman, and Joao Carreira. Perceiver: General perception with iterative attention. In *International conference on machine learning*, pages 4651–4664. PMLR, 2021. 2
- [18] Jungo Kasai, Keisuke Sakaguchi, Ronan Le Bras, Dragomir Radev, Yejin Choi, and Noah A Smith. A call for clarity in beam search: How it works and when it stops. In *Proceedings of the 2024 Joint International Conference on Computational Linguistics, Language Resources and Evaluation (LREC-COLING 2024)*, pages 77–90, 2024. 1
- [19] Lei Ke, Wenjie Pei, Ruiyu Li, Xiaoyong Shen, and Yu-Wing Tai. Reflective decoding network for image captioning. In *Proceedings of the IEEE/CVF international conference on computer vision*, pages 8888–8897, 2019. 2
- [20] Levon Khachatryan, Andranik Movsisyan, Vahram Tadevosyan, Roberto Henschel, Zhangyang Wang, Shant Navasardyan, and Humphrey Shi. Text2video-zero: Text-to-image diffusion models are zero-shot video generators. In *Proceedings of the IEEE/CVF International Conference on Computer Vision*, pages 15954–15964, 2023. 2
- [21] Philipp Koehn and Rebecca Knowles. Six challenges for neural machine translation. In *Proceedings of the First Workshop on Neural Machine Translation, NMT@ACL 2017, Vancouver, Canada, August 4, 2017*, pages 28–39. Association for Computational Linguistics, 2017. 1
- [22] Jing Yu Koh, Daniel Fried, and Russ Salakhutdinov. Generating images with multimodal language models. In *Advances in Neural Information Processing Systems 36: Annual Conference on Neural Information Processing Systems 2023, NeurIPS 2023, New Orleans, LA, USA, December 10 - 16, 2023*, 2023. 2, 5, 6
- [23] Hezheng Lin, Xing Cheng, Xiangyu Wu, and Dong Shen. Cat: Cross attention in vision transformer. In *2022 IEEE international conference on multimedia and expo (ICME)*, pages 1–6. IEEE, 2022. 2
- [24] Yuan Liu, Cheng Lin, Zijiao Zeng, Xiaoxiao Long, Lingjie Liu, Taku Komura, and Wenping Wang. Syncdreamer: Generating multiview-consistent images from a single-view image. 2024. 2
- [25] Yujie Lu, Pan Lu, Zhiyu Chen, Wanrong Zhu, Xin Wang, and William Yang Wang. Multimodal procedural planning via dual text-image prompting. In *Findings of the Association for Computational Linguistics: EMNLP 2024, Miami, Florida, USA, November 12-16, 2024*, pages 10931–10954. Association for Computational Linguistics, 2024. 17

- [26] Richard E. Mayer. Multimedia learning. pages 85–139. Academic Press, 2002. 17
- [27] Clara Meister, Gian Wiher, and Ryan Cotterell. On decoding strategies for neural text generators. *Trans. Assoc. Comput. Linguistics*, 10:997–1012, 2022. 2
- [28] Xichen Pan, Pengda Qin, Yuhong Li, Hui Xue, and Wenhua Chen. Synthesizing coherent story with auto-regressive latent diffusion models. In *Proceedings of the IEEE/CVF Winter Conference on Applications of Computer Vision*, pages 2920–2930, 2024. 2
- [29] Dustin Podell, Zion English, Kyle Lacey, Andreas Blattmann, Tim Dockhorn, Jonas Müller, Joe Penna, and Robin Rombach. SDXL: improving latent diffusion models for high-resolution image synthesis. 2024. 1
- [30] Jordi Pont-Tuset, Jasper Uijlings, Soravit Changpinyo, Radu Soricut, and Vittorio Ferrari. Connecting vision and language with localized narratives. In *Computer Vision—ECCV 2020: 16th European Conference, Glasgow, UK, August 23–28, 2020, Proceedings, Part V 16*, pages 647–664. Springer, 2020. 2
- [31] Tanzila Rahman, Hsin-Ying Lee, Jian Ren, Sergey Tulyakov, Shweta Mahajan, and Leonid Sigal. Make-a-story: Visual memory conditioned consistent story generation. In *Proceedings of the IEEE/CVF Conference on Computer Vision and Pattern Recognition*, pages 2493–2502, 2023. 2
- [32] Vasco Ramos, Yonatan Bitton, Michal Yarom, Idan Szpektor, and Joao Magalhaes. Contrastive sequential-diffusion learning: Non-linear and multi-scene instructional video synthesis. In *Proceedings of the Winter Conference on Applications of Computer Vision (WACV)*, pages 4645–4654, 2025. 1, 2, 3, 4, 5, 6, 12
- [33] Machel Reid, Nikolay Savinov, Denis Teplyashin, Dmitry Lepikhin, Timothy P. Lillicrap, Jean-Baptiste Alayrac, Radu Soricut, Angeliki Lazaridou, Orhan Firat, Julian Schrittwieser, Ioannis Antonoglou, Rohan Anil, Sebastian Borgeaud, Andrew M. Dai, Katie Millican, Ethan Dyer, Mia Glaese, Thibault Sottiaux, Benjamin Lee, Fabio Viola, Malcolm Reynolds, Yuanzhong Xu, James Molloy, Jilin Chen, Michael Isard, Paul Barham, Tom Hennigan, Ross McIlroy, Melvin Johnson, Johan Schalkwyk, Eli Collins, Eliza Rutherford, Erica Moreira, Kareem Ayoub, Megha Goel, Clemens Meyer, Gregory Thornton, Zhen Yang, Henryk Michalewski, Zaheer Abbas, Nathan Schucher, Ankesh Anand, Richard Ives, James Keeling, Karel Lenc, Salem Haykal, Siamak Shakeri, Pranav Shyam, Aakanksha Chowdhery, Roman Ring, Stephen Spencer, Eren Sezener, and et al. Gemini 1.5: Unlocking multimodal understanding across millions of tokens of context. *CoRR*, abs/2403.05530, 2024. 5
- [34] Robin Rombach, Andreas Blattmann, Dominik Lorenz, Patrick Esser, and Björn Ommer. High-resolution image synthesis with latent diffusion models. In *Proceedings of the IEEE/CVF conference on computer vision and pattern recognition*, pages 10684–10695, 2022. 1, 2
- [35] Olaf Ronneberger, Philipp Fischer, and Thomas Brox. U-net: Convolutional networks for biomedical image segmentation. In *Medical image computing and computer-assisted intervention—MICCAI 2015: 18th international conference, Munich, Germany, October 5-9, 2015, proceedings, part III 18*, pages 234–241. Springer, 2015. 2
- [36] Alexander M. Rush, Sumit Chopra, and Jason Weston. A neural attention model for abstractive sentence summarization. In *Proceedings of the 2015 Conference on Empirical Methods in Natural Language Processing, EMNLP 2015, Lisbon, Portugal, September 17-21, 2015*, pages 379–389. The Association for Computational Linguistics, 2015. 1
- [37] Chitwan Saharia, William Chan, Saurabh Saxena, Lala Li, Jay Whang, Emily L Denton, Kamyar Ghasemipour, Raphael Gontijo Lopes, Burcu Karagol Ayan, Tim Salimans, et al. Photorealistic text-to-image diffusion models with deep language understanding. *Advances in neural information processing systems*, 35:36479–36494, 2022. 1
- [38] Tim Salimans, Andrej Karpathy, Xi Chen, and Diederik P. Kingma. Pixelcnn++: Improving the pixelcnn with discretized logistic mixture likelihood and other modifications. 2017. 2
- [39] F. Serafini and J.P. Gee. *Reading the Visual: An Introduction to Teaching Multimodal Literacy*. Teachers College Press, 2014. 17
- [40] Chufan Shi, Haoran Yang, Deng Cai, Zhisong Zhang, Yifan Wang, Yujiu Yang, and Wai Lam. A thorough examination of decoding methods in the era of llms. In *Proceedings of the 2024 Conference on Empirical Methods in Natural Language Processing, EMNLP 2024, Miami, FL, USA, November 12-16, 2024*, pages 8601–8629. Association for Computational Linguistics, 2024. 2, 8
- [41] Marko Smilevski, Ilija Lalkovski, and Gjorgji Madjarov. Stories for images-in-sequence by using visual and narrative components. In *ICT Innovations 2018. Engineering and Life Sciences: 10th International Conference, ICT Innovations 2018, Ohrid, Macedonia, September 17–19, 2018, Proceedings 10*, pages 148–159. Springer, 2018. 2
- [42] Jascha Sohl-Dickstein, Eric Weiss, Niru Maheswaranathan, and Surya Ganguli. Deep unsupervised learning using nonequilibrium thermodynamics. In *International conference on machine learning*, pages 2256–2265. PMLR, 2015. 1
- [43] Jiaming Song, Chenlin Meng, and Stefano Ermon. Denoising diffusion implicit models. In *9th International Conference on Learning Representations, ICLR 2021, Virtual Event, Austria, May 3-7, 2021*. OpenReview.net, 2021. 1
- [44] Raphael Tang, Linqing Liu, Akshat Pandey, Zhiying Jiang, Gefei Yang, Karun Kumar, Pontus Stenetorp, Jimmy Lin, and Ferhan Ture. What the DAAM: interpreting stable diffusion using cross attention. In *Proceedings of the 61st Annual Meeting of the Association for Computational Linguistics (Volume 1: Long Papers), ACL 2023, Toronto, Canada, July 9-14, 2023*, pages 5644–5659. Association for Computational Linguistics, 2023. 2, 12
- [45] Ashwin Vijayakumar, Michael Cogswell, Ramprasaath Selvaraju, Qing Sun, Stefan Lee, David Crandall, and Dhruv Batra. Diverse beam search for improved description of complex scenes. In *Proceedings of the AAAI Conference on Artificial Intelligence*, 2018. 2
- [46] Sam Wiseman and Alexander M. Rush. Sequence-to-sequence learning as beam-search optimization. In *Proceed-*

*ings of the 2016 Conference on Empirical Methods in Natural Language Processing, EMNLP 2016, Austin, Texas, USA, November 1-4, 2016*, pages 1296–1306. The Association for Computational Linguistics, 2016. [4](#)

- [47] Yonghui Wu, Mike Schuster, Zhifeng Chen, Quoc V. Le, Mohammad Norouzi, Wolfgang Macherey, Maxim Krikun, Yuan Cao, Qin Gao, Klaus Macherey, Jeff Klingner, Apurva Shah, Melvin Johnson, Xiaobing Liu, Lukasz Kaiser, Stephan Gouws, Yoshikiyo Kato, Taku Kudo, Hideto Kazawa, Keith Stevens, George Kurian, Nishant Patil, Wei Wang, Cliff Young, Jason Smith, Jason Riesa, Alex Rudnick, Oriol Vinyals, Greg Corrado, Macduff Hughes, and Jeffrey Dean. Google’s neural machine translation system: Bridging the gap between human and machine translation. *CoRR*, abs/1609.08144, 2016. [1](#)

## A. Impact of Latent Selection on Beam Search Performance

Latent selection plays a crucial role in determining the quality and coherence of image sequences generated through beam search. By analyzing how different latent groups contribute to generation performance, we can better understand their impact on semantic alignment and visual coherence. To investigate this, we evaluate 15 tasks, each consisting of four steps, allowing us to systematically assess the effects of latent selection across a diverse set of sequences. Using both automatic evaluation and human annotations, we analyze different latent configurations to determine which groups contribute most to generating coherent and semantically meaningful sequences.

### A.1. Impact of Latent Groups on Performance

**Annotations.** Following the initial analysis of beam search configurations (Sec. 5.2), we further investigated the impact of using different latent configurations on the generated sequences. While latents 0, 1, 2 and 3 show promising results, latents 1, 3, 5, and 7 exhibit significantly poorer performance. For these latents, the beam search configurations yield very limited selection rates, indicating that they are rarely selected in both human and Gemini annotations. Specifically, for human annotations evaluated across 6 tasks, the only meaningful result is from the configuration with 4 steps back and a beam width of 3, achieving a selection rate of 8.33%. Other configurations show no selection rates.



Figure 8. Impact of using 1, 3, 5, and 7 latent configurations on image generation.

Similarly, for Gemini annotations evaluated on the same 6 tasks, the configurations do not yield any notable results, with no selection rates. When the evaluation is extended to 35 tasks, the performance for latents 1, 3, 5, and 7 re-

mains sparse, with a single configuration (2 steps back, beam width of 3) being selected, with a selection rate of 2.86%. Figure 8 visually demonstrates the poor results, where the images appear nearly identical, further supporting the findings of limited diversity and low performance, which aligns with the findings of [4, 32].

**Automatic Metrics.** Given the negative impact of higher latents on performance, as observed in human annotations, we decided to investigate the underlying reasons for this trend. Specifically, we explored how latents affect text-image alignment using the DAAM (Diffusion Attention Attribution Map) framework [44]. DAAM helps interpret text-to-image diffusion models by analyzing the cross-attention maps within the denoising process. It generates heat maps that highlight how much each token in the prompt influences different parts of the generated image, offering a visual representation of text-image alignment. By applying DAAM, we aimed to determine whether higher latents distort or weaken the contribution of key tokens during generation.

We then used DAAM to analyze the cross-attention between the input tokens and the generated image. DAAM enables us to track how much each remaining token influences specific regions of the image by calculating the attention patterns in the model. The resulting heat maps visualize this influence, with the intensity of the heat maps indicating the level of contribution each token has on different parts of the generated image. This approach helps us understand how well the model attends to key parts of the prompt and ensures that the most meaningful tokens are appropriately reflected in the image.

To quantify text alignment, we calculated the average heat map maximum intensity for all remaining tokens, providing a numerical measure of how well the model preserved the key textual elements in the generated image. Then, for each sequence of generated images, we computed the average alignment score across all images in the sequence. While this serves as an objective metric for evaluating text adherence, it remains a partial measure, as it focuses solely on text alignment without accounting for other important aspects of image quality, such as coherence, realism, or artistic fidelity. Figure 9 shows the average impact of different latent groups on text alignment. The results reveal a clear pattern, latents from earlier iterations contribute more effectively to aligning the text with the generated image, while text alignment weakens as we move to higher latent ranges. Specifically, latents in the 0–3 range showed the strongest alignment, with an average score of 1.544, followed by the 4–7 range (1.523) and the 8–11 range (1.435). In contrast, latents from the highest index range (16–19) had the weakest influence on alignment, with a significant drop in average scores. This suggests that earlier-stage la-

tents play a crucial role in preserving text fidelity, whereas later-stage latents may dilute or distort the contribution of key tokens.

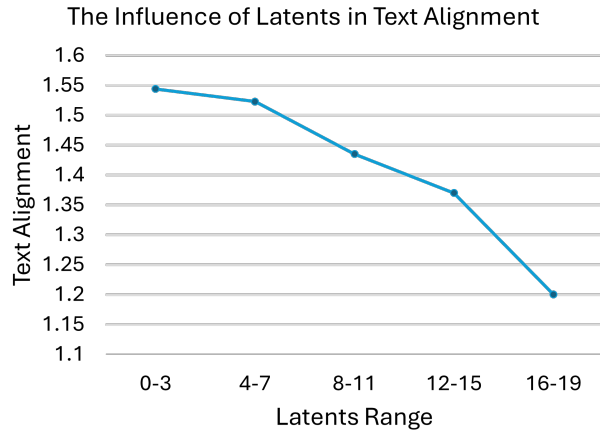


Figure 9. The average influence of latent indices on text alignment across task data.

In Figure 15, we analyze text alignment across multiple steps using heat maps corresponding to different latent groups, revealing how the connection between the input text and the generated image evolves throughout the process. Certain areas, such as the background and the bowl, show little to no heat map activation, indicating that these regions are less influenced by the text and more shaped by the model’s learned priors and overall scene composition. Since the model generates new images by building on latents from previous steps, these early decisions about text relevance persist throughout the process, influencing later refinements. Additionally, when examining generations using later latent groups, we find that this information remains more stable across all steps. This suggests that latents at these stages carry more structural and stylistic details, focusing on consistency rather than continuous adjustments based on the input text.

While later latents are effective at preserving visual consistency from previous steps, they are less capable of incorporating new details from the input prompts. For example, later latent groups (4-7) maintain stability in visual elements throughout the process, preserving previously established features. However, this comes at the expense of adapting to new or changing textual instructions. In contrast, early latent groups (0-3) demonstrate strong alignment between the text and the generated image, with consistently high heat map intensity across all steps. This highlights their role in grounding the image in the input text. For later latent groups (4-7), however, we observe a drop in heat map intensity, particularly by step 3, suggesting the model shifts focus away from strict textual adherence and toward refining finer vi-

sual details.

## A.2. Latent Selection on Image Sequence Generation

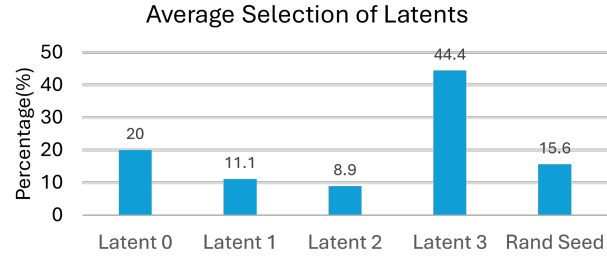


Figure 10. The average number of times that the model selected a given **latent** to generate the next image.

Following our evaluation of the impact of latent groups on performance, we now examine the influence of individual latents within the groups that exhibit better text alignment (0-3). As shown in Figure 10, Latent 3 is used most frequently, accounting for 44.4% of selections, followed by Latent 0 at 20%. In contrast, Latents 1 and 2 are used less often, with Latent 1 at 11.1% and Latent 2 at 8.9%. This uneven distribution suggests that Latents 0 and 3 are particularly effective at capturing key features at critical points in the generation process, which beam search exploits to enhance sequence coherence. The “Rand seed,” which introduces variability into the process, accounts for 15.6% of selections. This highlights beam search’s flexibility, allowing it to explore a range of possible outputs while preserving the overall structure of the image sequence.

In general, these findings reinforce the importance of latent selection strategies in optimizing image generation, suggesting that models could benefit from prioritizing the most impactful latents to achieve both coherent visual sequences and stronger text-image alignment.

Figure 11 illustrates the impact of different latent search methods on text alignment. The heat maps reveal how attention patterns shift based on the chosen decoding strategy, highlighting the differences in how each approach preserves or redistributes focus on textual cues throughout the image generation process. As shown, particularly in step 3, BeamDiffusion demonstrates superior text alignment compared to the other methods. Not only does it maintain a stronger connection to the input text, it also ensures better overall sequence coherence. This improved alignment and consistency across generations are key advantages of BeamDiffusion.

These variations provide further insight into how latent search methods can influence both the coherence of the generated sequence and the alignment between the input text and visual output.

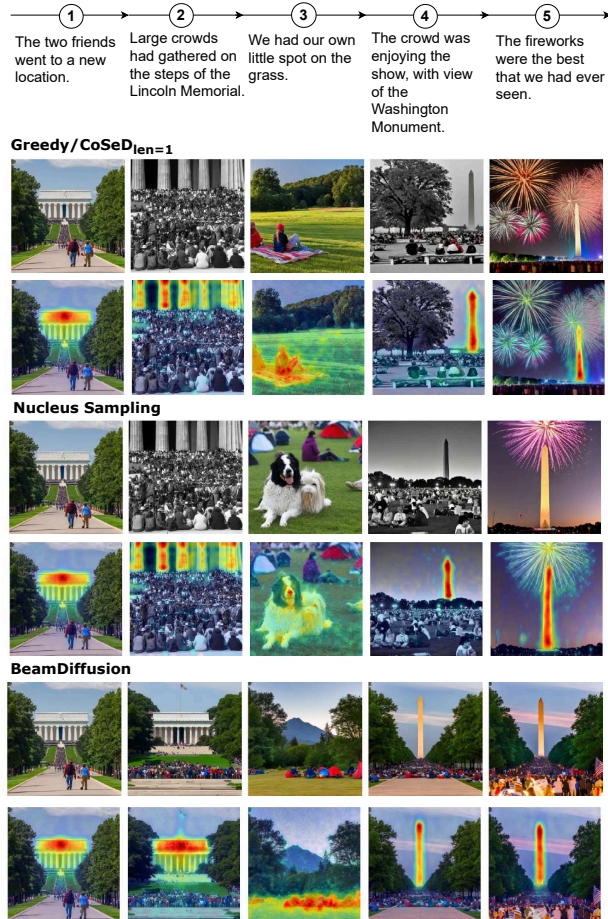


Figure 11. Heat maps illustrating cross-attention in latent diffusion across different decoding methods. The visualizations show variations in how each approach preserves or redistributes attention to textual cues throughout the generation process.

## B. Minimizing Decoding Risk

The generation process using diffusion models begins with a seed that determines the initial conditions of the model. The choice of this seed significantly affects the outcome, as it influences the path the model takes during generation. Using multiple random seeds in the first step ensures a diverse exploration of possible outputs, avoiding premature narrowing of options into a single path based on that seed. This limits the diversity of the results and increases the chance of missing better options.

**Greedy Decoding and Nucleus Sampling.** In both greedy decoding and nucleus sampling, we use the same approach in the first step. Multiple random seeds are employed to generate a set of candidate images. Each candidate is then evaluated using the CLIP score mechanism, which compares the generated images with the step text.

The image that best aligns with the text, according to the CLIP score, is selected to continue the process. This method ensures that both greedy decoding and nucleus sampling benefit from multiple diverse starting points, increasing the quality and variety of the generated outputs.

**BeamDiffusion.** In BeamDiffusion, relying on a single random seed in the first step effectively makes the process a greedy selection, as it locks the generation into a specific path. This limits diversity and reduces the chances of discovering higher-quality outputs. By using multiple random seeds, each seed generates a different decoding trajectory, helping to broaden the search space and increasing the likelihood of finding better solutions. Using multiple random seeds in the initial step enhances the exploration of the latent space, ensuring better and more diverse results across different decoding strategies.

**Random Seeds for mid-sequence Generation.** The sequence of scenes  $S = \{s_1, s_2, \dots, s_l\}$  may have one scene in the middle of the sequence that should be independent. To address this, for steps  $j > 1$ , we use a combination of random seeds and past latent vectors to maintain a balance between diversity and coherence, which is particularly important for such scenarios.

## C. Annotation Tasks

**Human annotations.** To facilitate the selection of the best beam search configuration, we developed a custom website specifically for human annotation. We found that existing tools lacked the flexibility necessary for our specific use case, especially when evaluating multiple configurations simultaneously. To select the best beam search configuration, 5 annotators are presented with 24 different sequences, each corresponding to a unique beam search configuration.

In total, the 24 configurations were generated by combining three key factors:

- **Steps Back:** This refers to how many previous steps the model uses from its latent representations to explore new candidate outputs. We evaluated three different settings for the number of steps back: 2, 3, and 4, which correspond to using latents from the last two, three, or four images, respectively.
- **Number of Latents:** We tested two sets of latent configurations  $\{1, 3, 5, 7\}$  and  $\{0, 1, 2, 3\}$  to explore how varying levels of latent detail impact the quality of the generated sequences.
- **Beam Width:** We explored four different beam widths  $\{2, 3, 4, 6\}$  which determine how many candidate sequences are retained at each step during the search process.

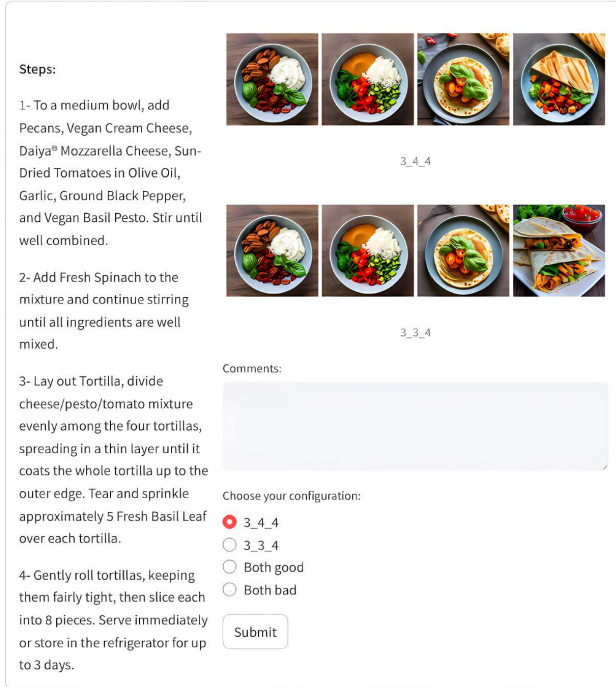


Figure 12. Example of the human annotation battle round for selecting the best beam search configuration.

Evaluating all of these at once proved to be exhausting and difficult to manage. To simplify the evaluation process, we adopted a "battle-style" annotation method. In this approach, 5 annotators compare two configurations at a time and select the one they find has better overall coherence. If neither configuration stands out, annotators can select "both good" or "both bad" (Figure 12), in which case the computationally cheaper option advances to the next round. This process is repeated until we identify the best configuration. This method focuses on direct comparisons, making it easier to pinpoint the most effective beam search settings while also considering computational efficiency.

To evaluate all models, 10 annotators are presented with four generated sequences side by side: one from the top-performing beam search configuration (selected during the initial annotations) and three others from alternative decoding methods, such as greedy search, nucleus sampling, and GILL. Figure 13 illustrates an example of this comparison process, where the annotators assess the sequences to determine the most effective approach.

**Gemini evaluation.** Figure 14 shows the prompt used in Gemini to annotate the best configuration and the best method. This prompt was used to guide the evaluation of image sequences based on visual and semantic consistency.

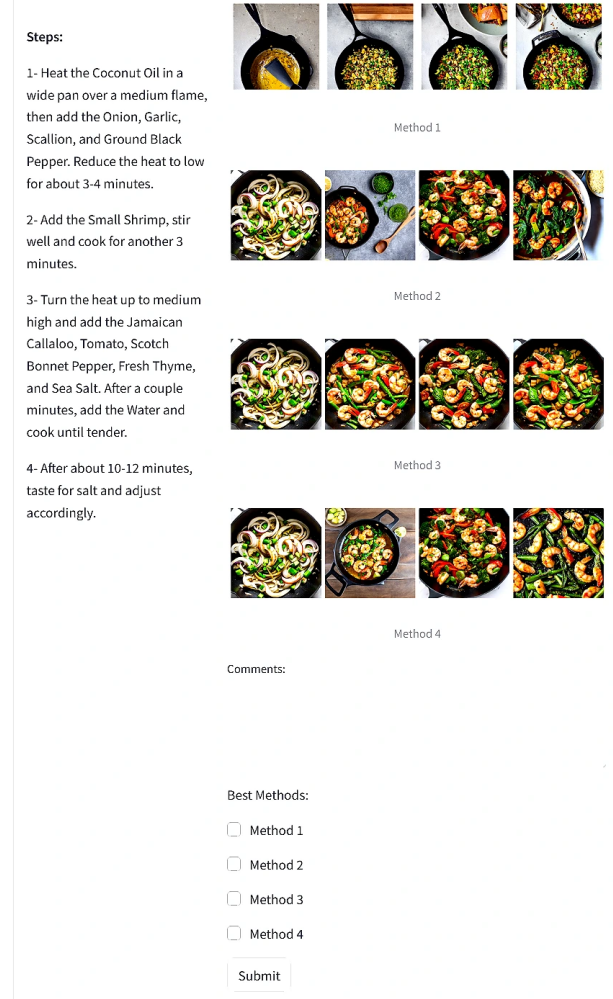


Figure 13. Example of a human annotation to choose the best decoding method.

## D. Datasets

**Recipes and DIYs.** Each manual task in both the Recipes and DIYs datasets includes a title, a description, a list of ingredients, resources and tools, and a sequence of step-by-step instructions, which may or may not be illustrated. The Recipes dataset comprises approximately 1,400 tasks, with an average of 4.9 steps per task, totaling 6,860 individual steps. Most tasks feature an image for each step. The DIYs dataset includes a variety of tasks, from simpler projects to more complex ones, with detailed steps.

**VIST.** We used the Descriptions of Images-in-Isolation (DII) annotations, as they allow for the generation of more precise and informative visual prompts. These annotations provide standalone descriptions of images, making it easier to capture their key visual elements without relying on sur-

**Gemini Prompt:**

”Evaluate two image sequences using the following criteria:

- **Visual Consistency:** Objects, ingredients, backgrounds, colors and styles should remain consistent across frames. Frames should transition smoothly, resembling a video-like progression with no sudden changes or missing elements.
- **Semantic Consistency:** Images must logically follow the described steps, clearly and accurately.

**Steps of the process:** {steps}

After evaluating all sequences, select the one with the strongest overall consistency (visual and semantic). Pay close attention to even minimal differences, as the sequences are very similar. If both sequences are equally good or bad, choose the one that is slightly better. Choose exactly one of the following options:

- ”First sequence”
- ”Second sequence” ”

Figure 14. Gemini prompt used to select the best beam search configuration and best method.

rounding context. The dataset includes 50 000 stories, offering a diverse range of visual and textual information. To ensure the most accurate and relevant annotation for each image, we leveraged CLIP. By using CLIP, we were able to select the annotation that best represented the image, improving the quality of our generated prompts and enhancing the overall alignment between text and visuals.

## E. Challenges

In the development and evaluation of the BeamDiffusion method, we encountered several challenges that required careful consideration and innovation. These challenges spanned multiple aspects of the model, ranging from the difficulty of generating accurate and concise captions, to identifying suitable domains for testing, and addressing the computational complexity of the generation process. While we were able to propose solutions for some of these challenges, others remain open and present ongoing areas of research. In this section, we outline the key challenges we faced and the strategies we employed, while acknowledging that not all of them have been fully addressed.

**Captions.** One of the challenges encountered in this process is generating captions that accurately describe the steps involved in the sequence. Often, a single step may consist of multiple sub-steps, each contributing to the overall generation. This makes it difficult to write a single concise caption that captures the full scope of each step. The challenge lies in ensuring that the caption not only reflects the specific action or transformation occurring at each stage but also conveys the progression and complexity of the entire sequence. Additionally, if we divide the steps into smaller sub-steps to better describe the process, the sequence becomes very extensive, making it even harder to maintain clarity and readability while ensuring comprehensive coverage of the entire generation process.

**Domains.** Identifying a domain that effectively highlights the advantages of the BeamDiffusion method, particularly the benefits of beam search, is still a challenge. While BeamDiffusion provides improvements in consistency and coherence, not all domains clearly showcase these advantages. Certain domains may lack the complexity or diversity needed to demonstrate the method’s strengths, such as its adaptive latent selection or its ability to maintain alignment with contextual instructions. Finding a domain that not only aligns with the method’s capabilities but also provides a clear and compelling demonstration of its improvements remains an ongoing challenge.

**Complexity of the generation.** The Beam Diffusion model generates multiple candidate images at each step by exploring a range of latents. We analyze the complexity of the model for a steps back of  $n$  steps and  $k$  latents explored. In the initial steps, the complexity is high because pruning begins only after the second step. For each beam,  $k \times n$  latents are explored, and the search space grows exponentially, resulting in significant computational cost in the early stages. During the first two steps, the complexity grows with the number of candidates and latents, proportional to  $O((k \times n)^j)$  for  $j \leq 2$ . Specifically, for  $j = 1$ , the complexity is proportional to the number of explored random seeds. After the second step, pruning reduces the number of candidates to the most promising  $w$  beams, decreasing the complexity to  $O(k \times n \times w)$ .

To further reduce complexity, a heuristic based on text relevance can be used to predict the top  $T$  most relevant past images. By restricting the search space to the latents of these top  $T$  candidates, the model improves efficiency by prioritizing contextually relevant images, particularly in the early steps. While the initial three steps remain computationally demanding due to the expansive search space, pruning combined with this heuristic can significantly lower



the computational cost by refining the candidate set.

## F. Application Examples

Images and other visual aids are essential tools that significantly improve comprehension in various fields. Whether while breaking down complex tasks, illustrating a sequence of events, or clarifying intricate concepts, visual representations provide clear, step-by-step guidance that makes the material easier to understand [26]. From technical procedures and instructional design to storytelling and educational content, the use of multiple-scene images allows the reader to grasp information more deeply and intuitively, transforming even the most complex or dense topics into something more accessible [11, 39]. However, generating a sequence of images that not only aligns with each textual instruction but also maintains overall coherence is a major challenge [25].

### F.1. Beam Search Tree

In Figure 16a, we provide another example of how the latent search occurs within the beam denoising process. This illustrates the BeamDiffusion model at work, showing the denoising of the initial seed to latents and how different beam paths are decoded. The figure highlights how our method explores the latent space, iterating through various latents based on the beam search strategy.

In Figure 16b, we observe that the generation of the selected image at step 4 behaves similarly to an isolated diffusion process. However, it is important to note that this process is influenced by multiple prompts. Specifically, the image generation at step 4 is conditioned on the prompts from steps 1, 3, and 4. This demonstrates how the latent search process incorporates context from various stages, showing that even though each generation step seems independent, it is shaped by previous steps, enabling a more coherent and consistent generation of the final image.

### F.2. Sequence Examples

To provide a comprehensive comparison between all models, we present several examples across different domains in Figures 17-28. These figures show case how each method performs in terms of maintaining sequence coherence throughout sequential image generation.

In our overall qualitative analysis, we observe that both Greedy/CoSeD<sub>len=1</sub> and Nucleus Sampling methods are generally good at following the textual input across steps, as shown in Figures 17, 20, 23, and 24. They align well with the step instructions but often struggle with visual consistency, as the generated images show noticeable shifts or inconsistencies between steps. This lack of visual cohesion detracts from the overall coherence of the sequence, even though they adhere reasonably well to the textual prompt. In contrast, GILL exhibits a different behavior. While it

maintains high visual consistency, with all images in the sequence being visually similar, it fails to accurately follow the step-by-step textual instructions. GILL tends to generate images that lack the necessary variability to incorporate new information from each step, resulting in sequences that are visually cohesive but contextually incorrect or incomplete.

Finally, BeamDiffusion strikes a strong balance between text adherence and visual consistency. As shown in Figures 17, 20, 23, and 24, it generally produces the most coherent sequences compared to other methods. In most cases, BeamDiffusion effectively follows the textual instructions while maintaining visual consistency across the steps. This combination of textual alignment and visual stability leads to more coherent and contextually accurate image sequences. While not without its limitations, BeamDiffusion demonstrates a more reliable progression throughout the image generation process than the other approaches. However, it is important to note that all methods face challenges in maintaining coherence within the DIY domain, as seen in Figures 25, 26, and 28. The complexity and diversity of DIY tasks present unique difficulties for the models, making it harder to both accurately follow textual instructions and ensure consistency throughout the sequence. While the models perform well in other domains, the intricacies of the DIY domain result in some inconsistencies, particularly when capturing step changes.

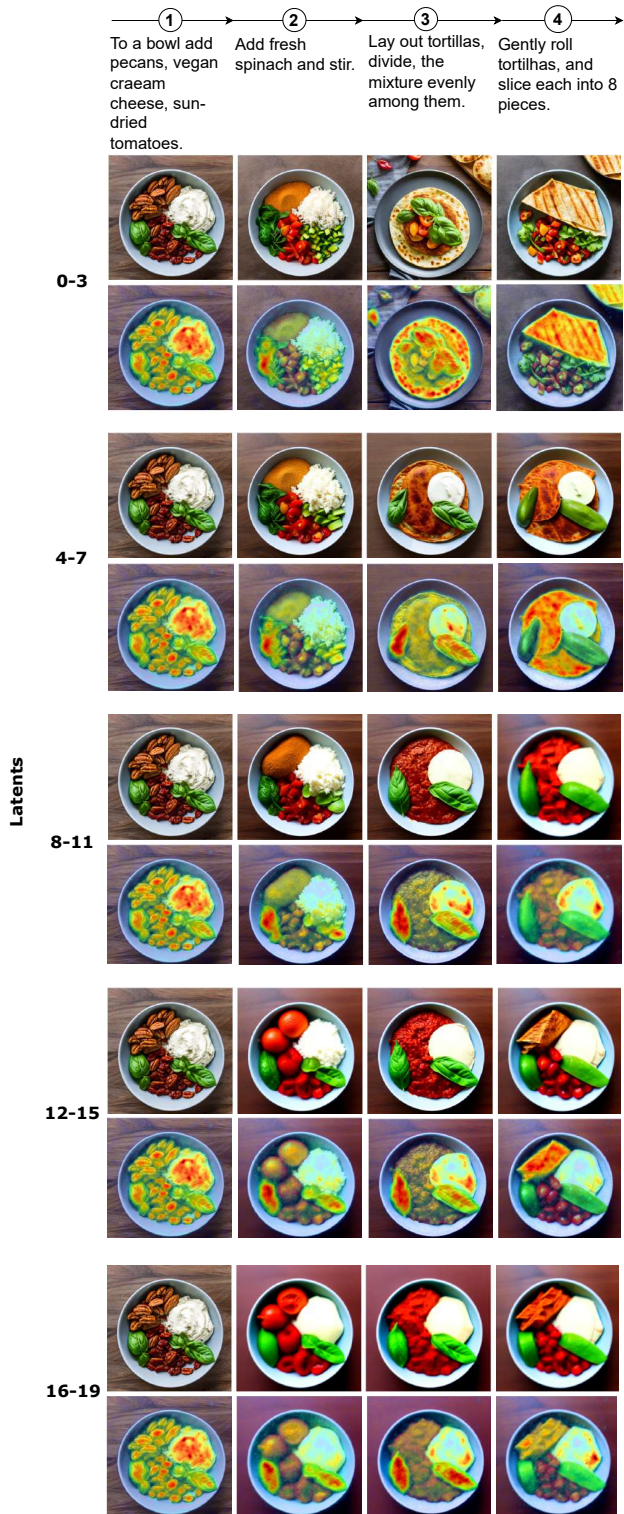
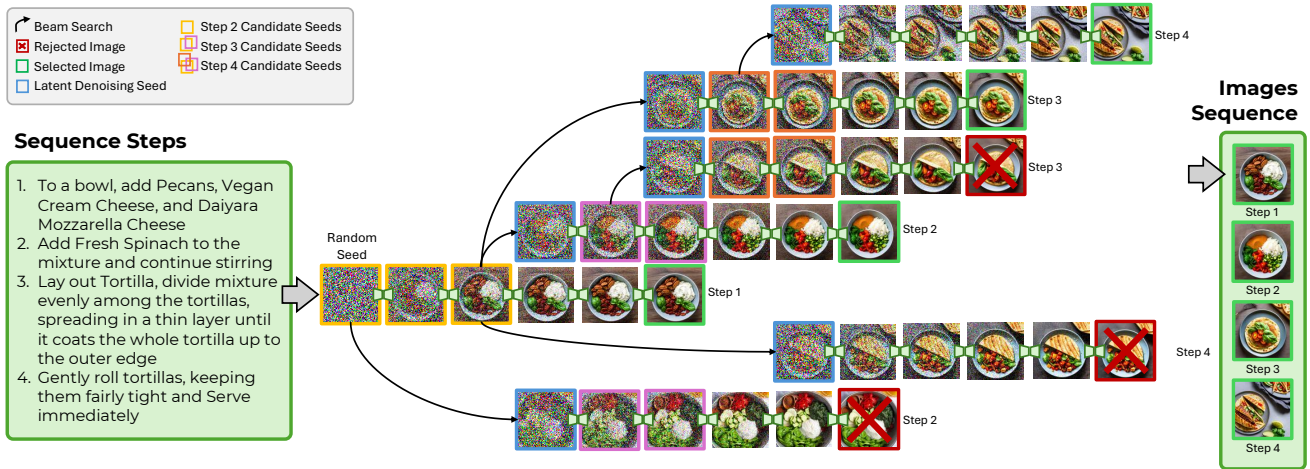
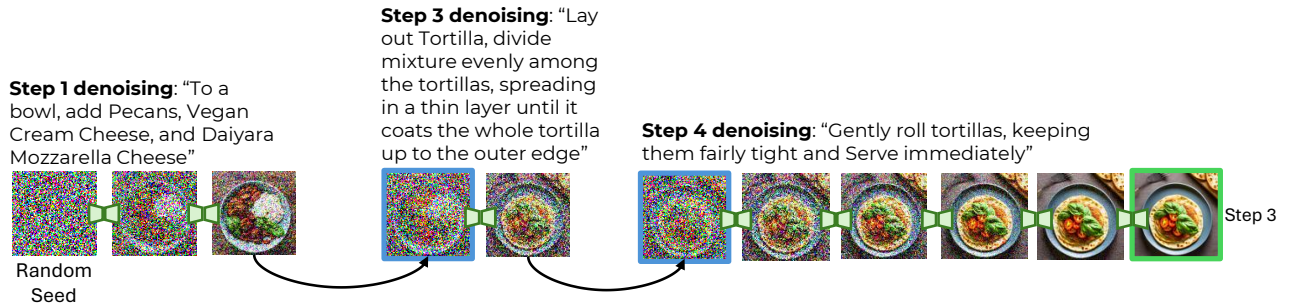


Figure 15. Visualization of cross-attention in latent diffusion across different sets of latents. The heat maps reveal how attention patterns evolve at various stages, highlighting the alignment between text prompts and distinct latent representations.



(a) The beam denoising search tree.



(b) Example of one complete decoded denoising process using contextual captions.

Figure 16. The beam diffusion model works in the denoising latent space by denoising the initial seed to latents and them decoding different beam paths. This shows how our method evolves in the latent space and how it can explore the latent space.

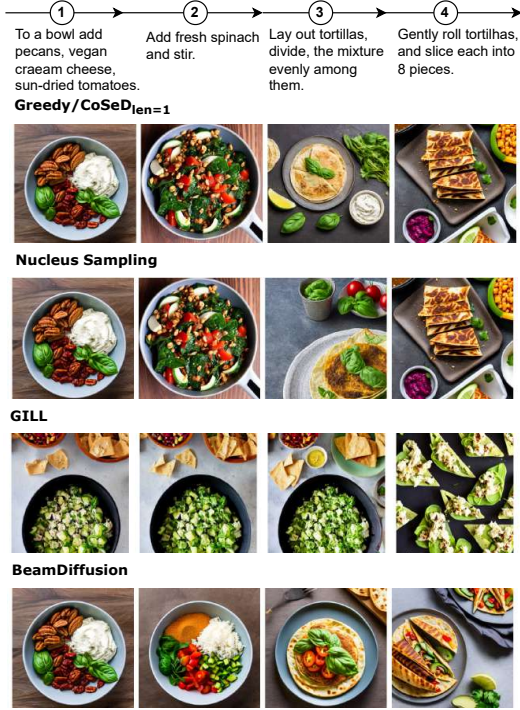


Figure 17. Example of the Recipes domain task "Vegan Basil Pesto and Sun-Dried Tomato Pinwheels", with a sequence of 4 steps.



Figure 19. Example of the Recipes domain task "Zucchini, Pecorino & Mint Salad", with a sequence of 4 steps.



Figure 18. Example of the Recipes domain task "Tangy lemon sheet cake", with a sequence of 4 steps.



Figure 20. Example of the Recipes domain task "Bone Broth", with a sequence of 3 steps.

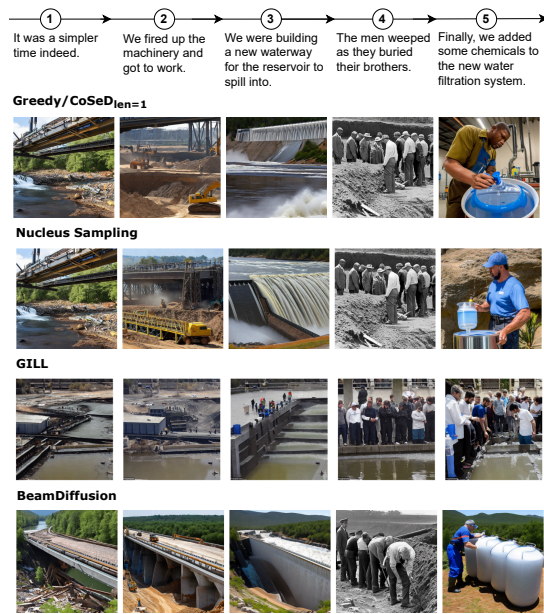


Figure 21. Example of the out-of-domain VIST story "Klamath Project Construction", with a sequence of 5 steps.

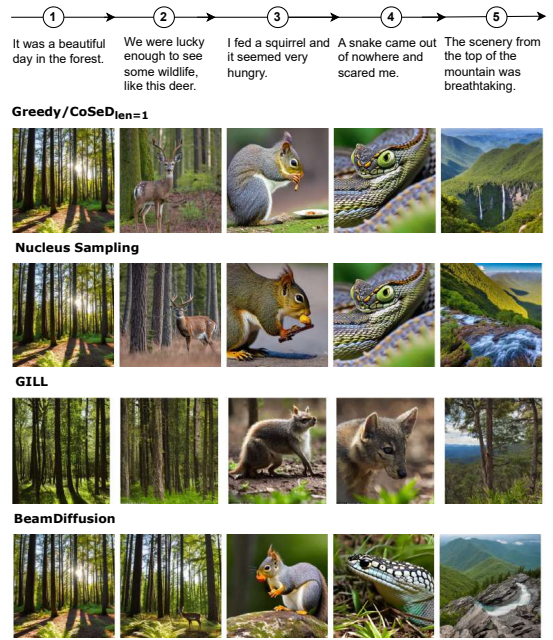


Figure 22. Example of the out-of-domain VIST story "Yosemite Weekend", with a sequence of 5 steps.

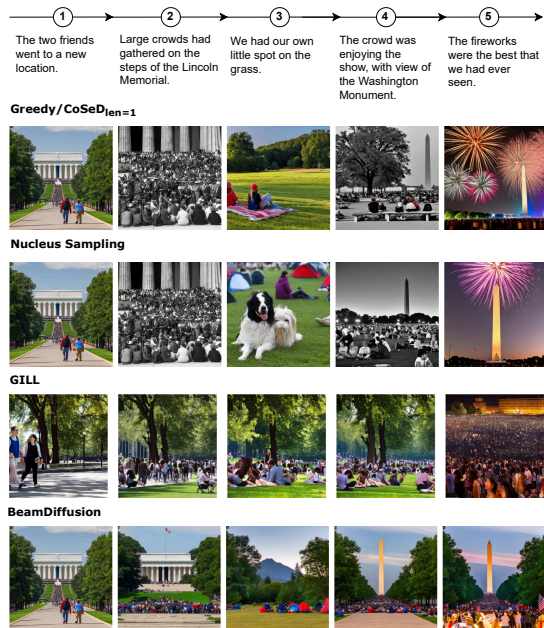


Figure 23. Example of the out-of-domain VIST story "Fireworks - 4th July in Washington, DC", with a sequence of 5 steps.

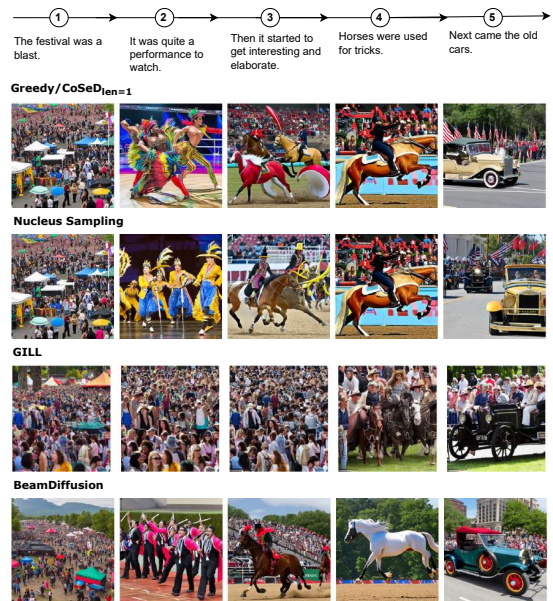


Figure 24. Example of the out-of-domain VIST story "Independence Day Parade", with a sequence of 5 steps.



Figure 25. Example of the out-of-domain DIY task "How to Clean Silk Rugs", with a sequence of 2 steps.



Figure 27. Example of the out-of-domain DIY task "How to Preserve Basil", with a sequence of 6 steps.



Figure 26. Example of the out-of-domain DIY task "How to Polish Wood", with a sequence of 3 steps.

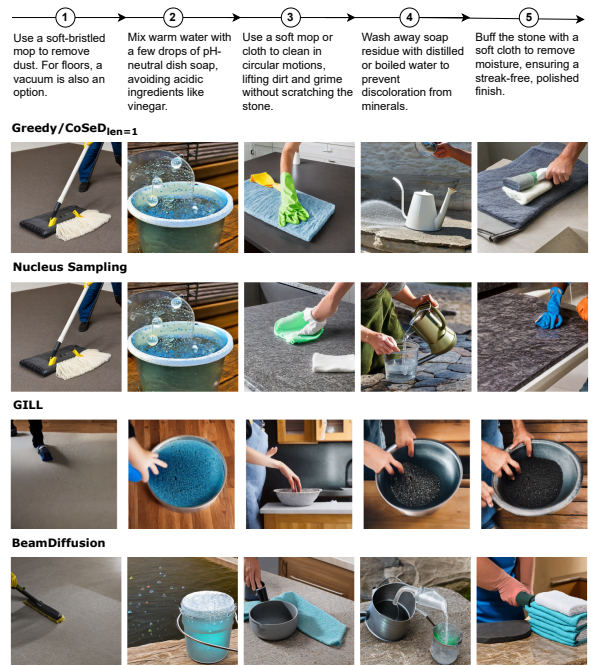


Figure 28. Example of the out-of-domain DIY task "How to Clean Natural Stone", with a sequence of 5 steps.